The International Journal of Advanced Manufacturing Technology (2019) 104:881–891
https://doi.org/10.1007/s00170-019-03888-8

ORIGINAL ARTICLE

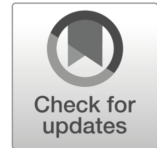

Finite element analysis of the effect of tool rake angle on brittle-to-ductile transition in diamond cutting of silicon

Junjie Zhang[1] · **La Han**[1] · **Jianguo Zhang**[2] · **Guo Li**[3] · **Jianfeng Xu**[2] · **Yongda Yan**[1] · **Tao Sun**[1]

Received: 4 January 2019 / Accepted: 20 May 2019 / Published online: 11 June 2019
© Springer-Verlag London Ltd., part of Springer Nature 2019

Abstract

Brittle-to-ductile transition plays a crucial role in ultra-precision machining of hard-brittle materials. In the present work, we investigate the brittle-to-ductile transition in diamond grooving of monocrystalline silicon by finite element modeling and simulation based on Drucker-Prager constitutive model. The brittle-to-ductile transition behavior is distinguished by analyzing evolutions of chip profile and cutting force. Corresponding diamond grooving experiment using the same machining configuration with the finite element simulation is also carried out to derive the critical depth of cut for the brittle-to-ductile transition. The comparison of experimental value of the critical depth of cut and predicted one by the finite element simulation demonstrates the high accuracy of as-established finite element model. Subsequent finite element simulations are performed to investigate the influence of rake angle of cutting tool on both diamond grooving and conventional diamond cutting with a constant depth of cut, which demonstrates a prominent dependence of brittle-to-ductile transition of silicon on the rake angle ranging from − 60° to 0°. And a critical rake angle for the most pronounced ductile machinability of silicon is found.

Keywords : Diamond cutting · Silicon · Brittle-to-ductile transition · Rake angle · Finite element simulation

1 Introduction

Silicon is a widely used semiconductor material in optoelectronic industries for its unique chemical, physical, and mechanical properties. For instance, monocrystalline silicon is the basic technological photovoltaic material for solar cells [1]. Ultra-precision optical machining is commonly applied to achieve ultimate surface finish of silicon, which has an important influence on the mechanical, optical, and electrical performance of silicon-based components and devices [2]. Ultra-precision single-point diamond turning (SPDT) has been demonstrated to be a powerful technique to achieve high-integrity mirror surface of non-ferrous metallic materials [3, 4]. However, achieving ultra-smooth surface of silicon by diamond cutting is challenging due to its low machinability, which is intrinsically associated with the hard-brittle characteristic accompanied by the strong covalent bonds [5].

It has been demonstrated that the ductile mode cutting of hard and brittle materials can be achieved by rational selection of machining parameters, such as cutting parameters, material orientation, and geometry of cutting tool [6–18]. For instance, the utilization of a negative rake angle of a diamond cutting tool leads to formation of local compressive hydrostatic pressure at the contact regime between workpiece material and cutting tool, which efficiently suppresses crack propagation and thus facilitates the material removal through plastic flow rather than brittle fracture [19, 20]. To achieve high surface integrity of silicon through ductile mode cutting, it is critical to obtain a fundamental understanding of underlying mechanisms governing the brittle-to-ductile (BTD) transition in diamond cutting of silicon, which also provide important guidelines for the rational development of cutting tools [21, 22].

Grooving experiments with gradually increasing depth of cut (DOC) have been popularly used to characterize the BTD

✉ Junjie Zhang
zhjj505@gmail.com

✉ Jianguo Zhang
zhangjg@hust.edu.cn

[1] Center for Precision Engineering, Harbin Institute of Technology, Harbin 150001, China

[2] State Key Laboratory of Digital Manufacturing Equipment and Technology, School of Mechanical Science and Engineering, Huazhong University of Science and Technology, Wuhan 430074, China

[3] Research Center of Laser Fusion, China Academy of Engineering Physics, Mianyang 621900, China

transition of different types of hard-brittle materials [23–26]. Specifically, the transition from ductile mode cutting at low DOC to brittle mode cutting at high DOC can be characterized by ex situ imaging the groove morphology with optical microscopy. Thus, a critical DOC for the BTD transition can be derived, which is greatly significant to determine the DOC used in subsequent ductile mode SPDT. However, it is extremely difficult to reveal underlying mechanisms of BTD transition by conventional experimental techniques due to the resolution limitations of both machining and measurement apparatus. Furthermore, although the direct and straightforward analysis of subsurface deformation behavior of silicon by state-of-the-art cross-sectional transmission electron microscopy (TEM) discovered new nanostructure in silicon in single grain grinding, it incurs a high cost and is time-consuming [27, 28]. On the other hand, as an important supplementary to experimental investigation, finite element (FE) simulation-based numerical investigation has been widely performed to investigate machining process of silicon [29–32].

Although considerable FE simulations have been performed to provide valuable insights into diamond cutting of silicon, an exhaustive description of the BTD transition of silicon by FE simulation is far from being completed. Firstly, while most of previous FE simulations adopted constant DOCs [29–32], there is limited attention paid to the FE simulation of grooving trial and its machining parameters' dependence. Furthermore, a quantitative comparison between experimental results and FE simulation prediction data in diamond grooving is still lacking. Moreover, while the BTD transition can be experimentally identified from various aspects such as groove profile [24–27], cutting force [25, 33], and acoustic emission signal [34, 35], the BTD transition in previous FE simulations is solely distinguished from the evolution of chip profile. Therefore, other theoretical aspects are also expected for providing robust evidence of the BTD transition in FE simulations. Furthermore, there are diverse constitutive models such as Johnson-Cook [29] and Von Mises yield criterion [36] used in previous FE simulations, which failed to provide accurate reflection of the brittle fracture behavior of silicon. Since proper description of material properties is critical for the accuracy of FE simulation results, it is prerequisite to adopt suitable constitutive model that can fully represent ductile and brittle characteristics of silicon for elucidating mechanisms of BTD transition.

Both theoretical and experimental studies indicate that diamond cutting of silicon is essentially an intricate process that includes elastic deformation, plastic deformation, brittle fracture, and phase transition, and the interaction between different deformation modes strongly relies on the configuration of machining parameters [37]. Specifically, the rake angle of the cutting tool is one of the most prominent machining parameters that are closely associated with the BTD transition in diamond cutting of silicon. It is normally accepted that the ductile mode cutting of silicon can mainly be achieved by using a cutting tool with negative rake angles [25–28]. Fang et al. [38] experimentally showed that the effective rake angle plays a more important role than nominal rake angle in cutting brittle materials. However, the consensus on the quantitative dependence of BTD transition of silicon on rake angle has not been reached. Zhao et al. [39] reported that the rake angle between − 25° and − 15° is suitable for achieving the ductile mode cutting of silicon. Krulewich et al. [37] concluded that the rake angle for ductile mode cutting of silicon should not exceed − 60°. Durazo-Cardenas et al. [40] pointed out that a rake angle of − 25° is the best conducive to achieve ductile cutting of silicon. Wang et al. [41] demonstrated that a rake angle of − 40° leads to better machined surface quality than a rake angle of − 25°. These discrepancies in the rake angle–dependent BTD transition of silicon may be originated from different configurations of utilized machining parameters. Therefore, revealing the rake angle–dependent BTD transition in diamond cutting of silicon by an accurate FE model is greatly needed.

Therefore, in the present work, we establish a FE model of diamond cutting of monocrystalline silicon based on the Drucker-Prager (DP) constitutive model, which is capable of capturing plastic flow and brittle fracture of silicon. We subsequently perform FE simulation of grooving to investigate the BTD transition of silicon by analyzing evolutions of both chip profile and cutting force. Furthermore, corresponding diamond grooving experiment using the same machining parameters with that used in the FE simulation is also carried out, and the derived critical DOC for the BTD transition is quantitatively compared with the predicted value by the FE simulation. Finally, sequential FE simulations of grooving and conventional cutting using a constant DOC are performed to investigate the influence of rake angle on the BTD transition of silicon.

2 Methodology

2.1 FE modeling of grooving of silicon

Figure 1 shows the 2D FE model of orthogonal grooving of silicon, which consists of a monocrystalline silicon specimen and a diamond cutting tool. The specimen has dimensions of 30 μm in length and 10 μm in height, and is meshed by CPE4R type element with an element size of 8 nm. To restrict rigid motion of the specimen in the cutting process, the specimen bottom is fully restricted. The diamond cutting tool treated as an analytical rigid body has a relief angle of 10° and a cutting edge radius of 40 nm. To address the influence of rake angle on the cutting process, five rake angles, as 0°, − 15°, − 30°, − 45°, and − 60°, respectively, are considered.

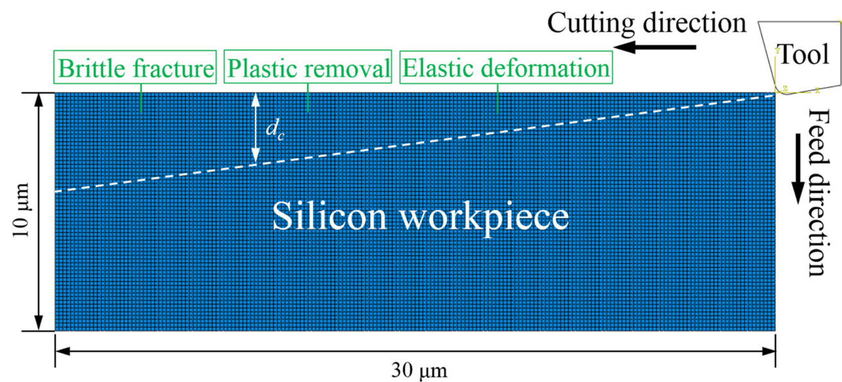

Fig. 1 2D FE model of orthogonal grooving of silicon

Prior to the cutting process, the cutting tool edge is placed above the right corner of the specimen with a distance of 5 nm. In the FE simulation of grooving process, the cutting tool moves with a constant speed of 30 mm/s and 3.6835 mm/s along the cutting direction and the DOC direction, respectively. The maximum cutting length and DOC of the grooving process are 2.44 and 0.3 μm, respectively. Correspondingly, the inclination angle of cutting tool trajectory with respect to the specimen top surface is 7°, as illustrated in Fig. 1. It is expected that the silicon material sequentially undergoes elastic deformation, plastic deformation, and brittle fracture upon the advancement of cutting tool. Specifically, plastic removal and brittle fracture dominate ductile mode cutting and brittle mode cutting, respectively.

The DP constitutive law is utilized to describe material properties of silicon in the FE simulation. Table 1 lists specific parameters of the DP constitutive law for silicon [42]. In addition, the unit failure criterion is adopted in the shear failure model based on the equivalent plastic strain value of the unit. The fracture strain of silicon is set as 0.01 [43].

2.2 Setup of grooving experiment

Figure 2 illustrates the experimental configuration of diamond grooving of silicon using a single-crystal diamond cutting tool. The workpiece is a mechanically polished monocrystalline Si(100) with a diameter of 30 mm, a thickness of 2 mm, and a surface roughness of 1 nm. Both the rake face and flank face of the diamond cutting tool have a (100) crystallographic orientation. The cutting tool with an arc-shaped cutting edge has a radius of 1 mm, a rake angle of − 15°, a relief angle of 25°, and a cutting edge radius of approximately 40 nm. The experiment is carried out with the Precitech Nanoform X ultra-precision lathe. The lathe has a linear position motion accuracy of 1 nm, which enables the precision reciprocating motion along cutting direction and feed direction. In the cutting process, the workpiece and cutting tool are fixed to the Z and X axes of the linear motion axis of the lathe, respectively. To be consistent with the FE simulation, in the grooving experiment, the cutting tool has a cutting speed of 30 mm/s and 3.6835 mm/s along the cutting direction and the DOC direction, respectively. Thus, the inclination angle of cutting tool trajectory with respect to the specimen top surface in the grooving experiment is 7°, which is the same with that in FE simulation. The machined surface is characterized by optical microscopy and scanning electron microscopy (SEM).

3 Results and discussion

3.1 BTD transition of silicon

FE simulation of grooving using a rake angle of − 15° is firstly carried out to investigate the BTD transition behavior of silicon. Figure 3 shows representative snapshots of cutting process at different cutting regimes, in which the specimen is colored by stress contour. As indicated by the scale bar shown in Fig. 3a, the height of the intercepted part from the specimen is 465 nm. Figure 3 a shows that in the initial cutting regime, the material undergoes pure plastic deformation without chip formation, and the stress mainly concentrates in the vicinity of tool edge. Upon further advancement of cutting tool, Fig. 3 b shows that there is continuous saw-tooth chip formed by plastic flow, i.e., ductile mode cutting. Figure 3 b shows that

Table 1 Parameters of DP constitutive law for silicon [42]

Parameters	Density (ton/mm^3)	Elastic modulus (MPa)	Poison's ratio	Initial yield (MPa)	Friction angle (°)	Dilation angle (°)	*K*
Values	2.3×10^{-9}	193000	0.28	7000	18	5	0.9

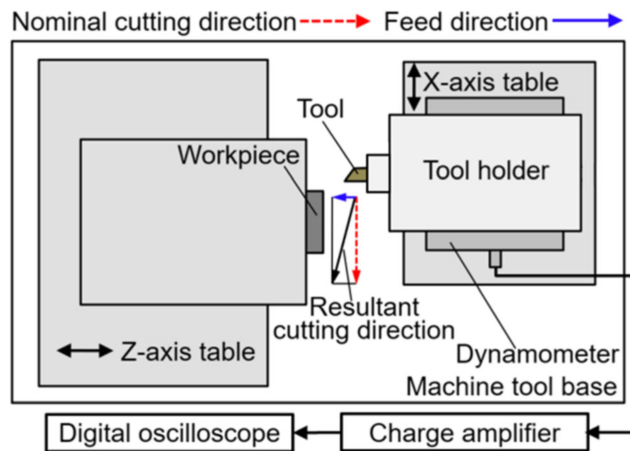

Fig. 2 Illustration of experimental configuration of grooving

cutting stress is mainly concentrated in the first deformation zone in the vicinity of the cutting edge. Figure 3 a also shows that the magnitude of stress increases with increasing DOC.

Operating ductile and/or brittle material removal of silicon is strongly dependent on the applied stress state. The generation of compressive stress around the tool-workpiece contacting zone prevents crack propagation due to the absence of tensile stress in the cleavage plane [12]. Liu et al. theoretically demonstrated that the compressive stressed zone acts as a shielding zone for crack propagation, because the stress intensity factor K at the crack tip is reduced by the large compressive stress. Consequently, material removal within the shielding zone is dominated by dislocation flow [6, 8, 25]. In addition to dislocation activity-governed plastic flow, phase transformation and amorphization occurred under highly compressive pressure also play an important role in the BTD transition of silicon [34–49]. Yan et al. [50] reported a combined effect of both phase transformation and dislocation motion on the ductile mode cutting of silicon. Zhang et al. [27, 51] found that the formation of amorphous layer before chip formation is also one important mechanism for ductile mode cutting of silicon in high-speed grinding experiments, and the critical DOC for BDT transition varies from 48.7 to 122.3 nm.

In addition to the stress concentration in the first deformation zone, Fig. 3 c indicates that the stress concentration is mainly retreated to the vicinity of cutting edge accompanied

Fig. 3 Evolution of chip profile in FE simulation of grooving with a rake angle of − 15°. Silicon specimen is colored by stress contour. **a** Plastic deformation. **b** Ductile mode cutting. **c** BTD transition region. **d** Brittle mode cutting

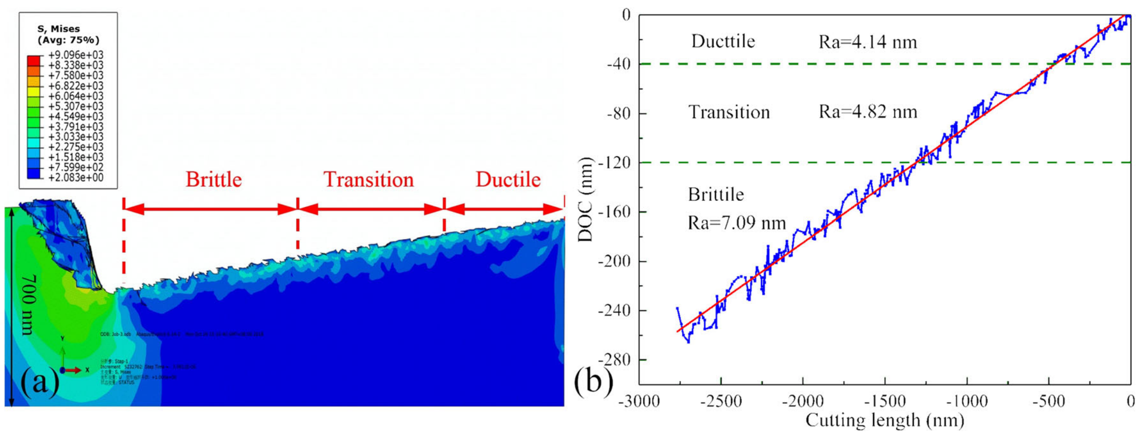

Fig. 4 Machined surface morphology after FE simulation of grooving with a rake angle of – 15°. **a** Machined surface morphology. Silicon specimen is colored by stress contour. **b** Variation of surface coordinates

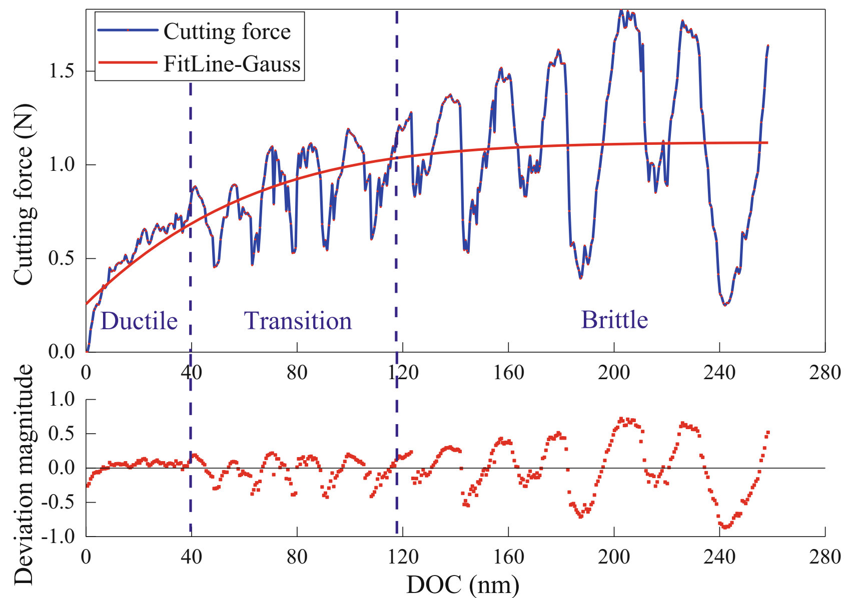

Fig. 5 Variation of cutting force in the FE simulation of grooving with a rake angle of − 15°

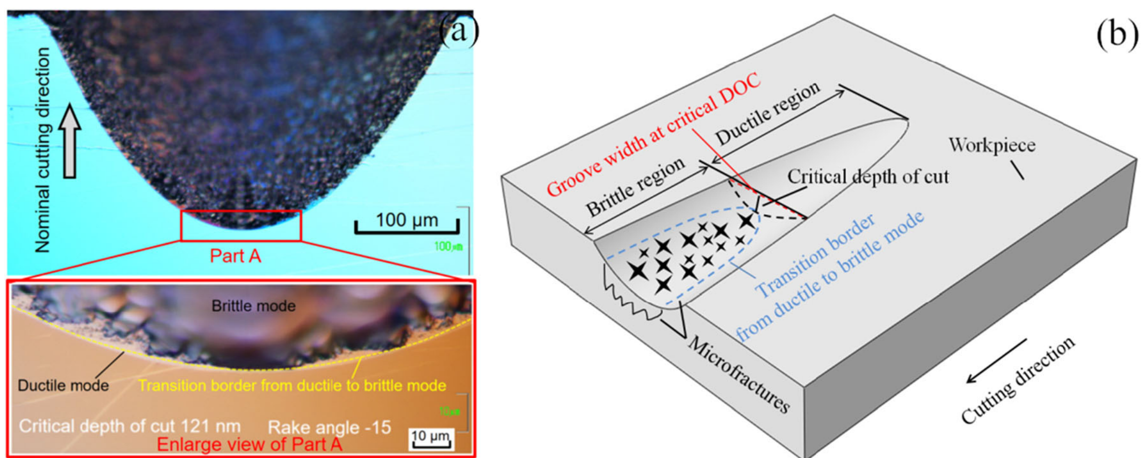

Fig. 6 **a** Top view of groove morphology. **b** Schematic of critical depth measurement

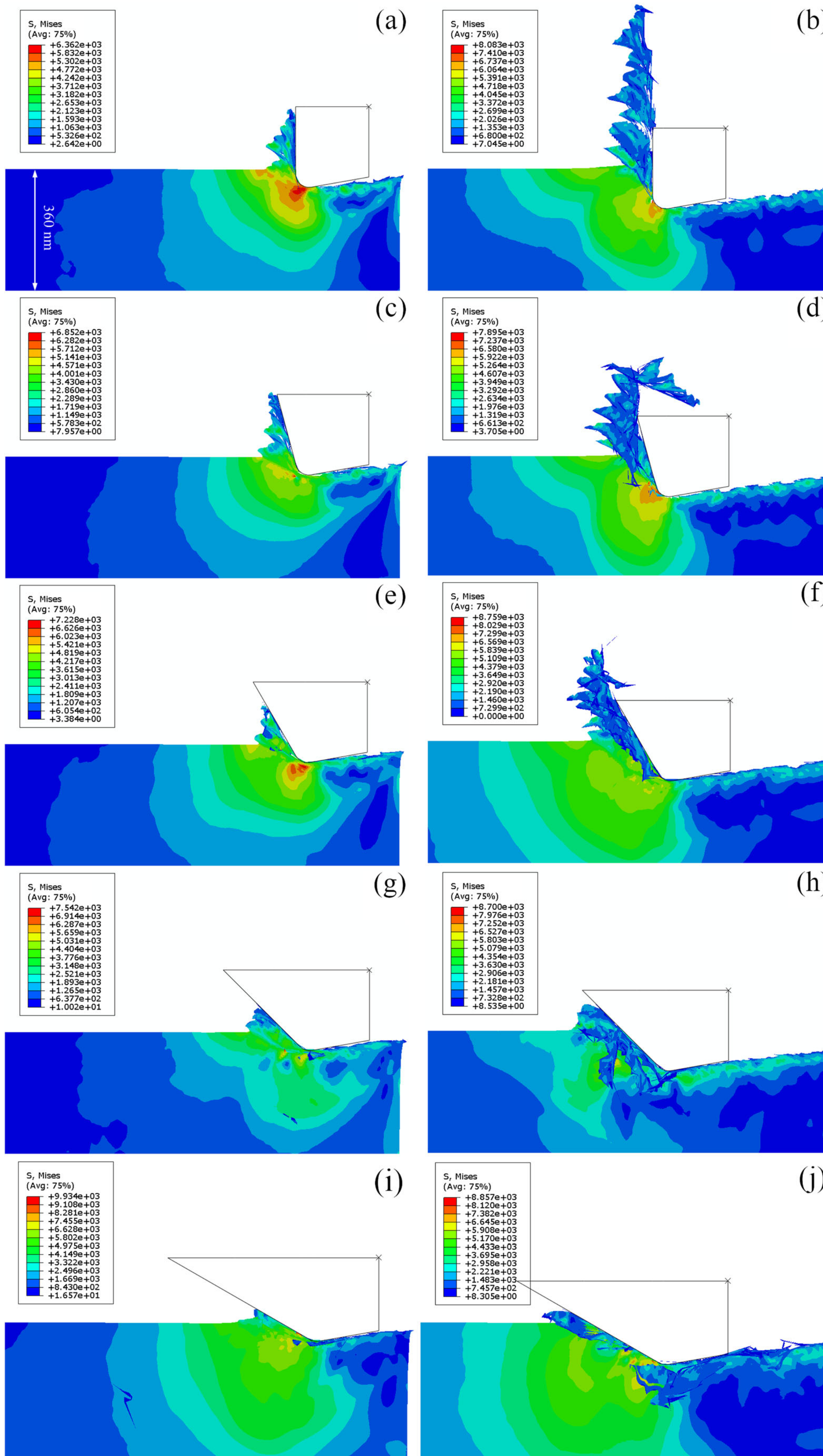
(a)
S, Mises
(Avg: 75%)
+6.362e+03
+5.832e+03
+5.302e+03
+4.772e+03
+4.242e+03
+3.712e+03
+3.182e+03
+2.653e+03
+2.123e+03
+1.593e+03
+1.063e+03
+5.326e+02
+2.642e+00
360 nm
(b)
S, Mises
(Avg: 75%)
+8.083e+03
+7.410e+03
+6.737e+03
+6.064e+03
+5.391e+03
+4.718e+03
+4.045e+03
+3.372e+03
+2.699e+03
+2.026e+03
+1.353e+03
+6.800e+02
+7.045e+00
(c)
S, Mises
(Avg: 75%)
+6.852e+03
+6.282e+03
+5.712e+03
+5.141e+03
+4.571e+03
+4.001e+03
+3.430e+03
+2.860e+03
+2.289e+03
+1.719e+03
+1.149e+03
+5.783e+02
+7.957e+00
(d)
S, Mises
(Avg: 75%)
+7.895e+03
+7.237e+03
+6.580e+03
+5.922e+03
+5.264e+03
+4.607e+03
+3.949e+03
+3.292e+03
+2.634e+03
+1.976e+03
+1.319e+03
+6.613e+02
+3.705e+00
(e)
S, Mises
(Avg: 75%)
+7.228e+03
+6.626e+03
+6.023e+03
+5.421e+03
+4.819e+03
+4.217e+03
+3.615e+03
+3.013e+03
+2.411e+03
+1.809e+03
+1.207e+03
+6.054e+02
+3.384e+00
(f)
S, Mises
(Avg: 75%)
+8.759e+03
+8.029e+03
+7.299e+03
+6.569e+03
+5.839e+03
+5.109e+03
+4.379e+03
+3.649e+03
+2.920e+03
+2.190e+03
+1.460e+03
+7.299e+02
+0.000e+00
(g)
S, Mises
(Avg: 75%)
+7.542e+03
+6.914e+03
+6.287e+03
+5.659e+03
+5.031e+03
+4.404e+03
+3.776e+03
+3.148e+03
+2.521e+03
+1.893e+03
+1.265e+03
+6.377e+02
+1.002e+01
(h)
S, Mises
(Avg: 75%)
+8.700e+03
+7.976e+03
+7.252e+03
+6.527e+03
+5.803e+03
+5.079e+03
+4.354e+03
+3.630e+03
+2.906e+03
+2.181e+03
+1.457e+03
+7.328e+02
+8.535e+00
(i)
S, Mises
(Avg: 75%)
+9.934e+03
+9.108e+03
+8.281e+03
+7.455e+03
+6.628e+03
+5.802e+03
+4.975e+03
+4.149e+03
+3.322e+03
+2.496e+03
+1.669e+03
+8.430e+02
+1.657e+01
(j)
S, Mises
(Avg: 75%)
+8.857e+03
+8.120e+03
+7.382e+03
+6.645e+03
+5.908e+03
+5.170e+03
+4.433e+03
+3.695e+03
+2.958e+03
+2.221e+03
+1.483e+03
+7.457e+02
+8.305e+00

◀ **Fig. 7** FE simulation results of grooving silicon using different rake angles. Silicon specimen is colored by stress contour. For each rake angle, left and right snapshots in the same row are captured at a DOC of 60 and 125 nm, respectively. Rake angles are the following: **a** and **b** 0°, **c** and **d** − 15°, **e** and **f** − 30°, **g** and **h** − 45°, **i** and **j** − 60°

with fracture failure of formed chips, i.e., BTD transition occurs. Figure 3 d shows that material removal is dominated by brittle fracture, i.e., brittle mode cutting. Therefore, the evolution of chip profile shown in Fig. 3 clearly demonstrates that BTD transition occurred in the grooving of silicon with increasing DOC. The critical DOC for the commencing of dominant brittle mode cutting is estimated as 118 nm.

Figure 4 a shows machined surface morphology of silicon after the FE simulation of grooving with a rake angle of − 15°. Furthermore, Fig. 4 b plots derived coordinates of machined surface in the entire grooving process, and the surface roughness of machined surface in different cutting regimes is also derived. Figure 4 a and b jointly demonstrate the significant evolution of machined surface quality in different cutting regimes. Specifically, the machined surface is smooth in the ductile mode cutting. The derived surface roughness is 4 nm. However, the machined surface quality deteriorates in the BTD transition regime. The cracks are generated on the machined surface, which leads to an increased surface roughness of 5 nm. Figure 4 a shows that there are pronounced fracture propagation phenomena formed in the brittle mode cutting with a surface roughness of 8 nm.

Figure 5 plots the variation of cutting force in the FE simulation of grooving process with a rake angle of − 15°. Furthermore, to qualitatively characterize the fluctuation of cutting force, the evolution of deviation magnitude of cutting force with DOC is also presented. The deviation magnitude of cutting force is calculated by subtracting the base number derived from the fitting of cutting force-DOC curve using the measured number. The thrust force that has the similar features with the cutting force is not presented. While a reference point is assigned to represent the analytical rigid cutting tool, both cutting force and thrust force can be directly derived from the reference point. Figure 5 demonstrates that there are different characteristics of cutting force in different cutting regimes. In the initial cutting regime with a DOC less than 40 nm, the cutting force increases smoothly with little deviation magnitude due to considerable shear bands formed in the saw-tooth chips. When the DOC is larger than 40 nm but less than 118 nm, the fluctuation of cutting force is significantly magnified. Although the amplitude of fluctuation increases with DOC, the deviation magnitude of cutting force nearly keeps constant, indicating a stable transition from ductile mode cutting to brittle mode cutting occurred. However, the evolution of deviation magnitude loses its regularity when the DOC is larger than 118 nm, as the fluctuation of cutting force aggravates significantly due to dominant brittle fracture events. Figure 5 also shows that the increasing ratio of averaged cutting force is slowed down in the brittle mode cutting. The above analysis further quantitatively confirms the critical DOC of 118 nm derived from the evolution of chip profile.

In addition to the FE simulation, corresponding grooving experiment using the same machining parameters with the FE simulation is carried out. Figure 6 a presents the top view of machined surface morphology of the formed groove, which clearly indicates a transition border of cutting mode from ductile to brittle. It should be noted that since a large inclination angle of 7° is utilized in the experiment, the ultra-small groove length of 2.44 μm is far smaller than that of hundreds of micrometers used in previous grooving experiments. Figure 6 b illustrates the scheme to derive the critical DOC from machined surface morphology. The critical DOC d_c in grooving experiment can be calculated following Eq. (1):

$$dc = R - \sqrt{R^2 - \left(w/2\right)^2} \tag{1}$$

where R is the nose radius of the diamond cutting tool and w is the width of the groove at the critical DOC. The critical DOC obtained in the grooving experiment is 121 nm. The deviation of critical DOC between predicted value by FE simulation and measured value in experiment is 2.4%, indicating the high accuracy of as-established FE model of grooving of silicon.

3.2 Influence of rake angle on BTD transition

With the fundamental understanding of the BTD transition of silicon in grooving by FE simulation and corresponding experimental validation, FE simulations of grooving using different rake angles are subsequently carried out to investigate the influence of rake angle of cutting tool on the BTD transition of silicon. In addition to the rake angle of − 15°, other four rake angles including 0°, − 30°, − 45°, and − 60° are considered. The machining parameters for the other four rake angles are the same as those used for the rake angle of − 15°.

Figure 7 presents snapshots of cutting processes with the same DOC for different rake angles, in which the specimen is colored by stress contour. For each rake angle, left-row and right-row snapshots correspond to a DOC of 60 and 125 nm, respectively. It is seen from Fig. 7 that there are continuous chips formed for each rake angle at the DOC of 60 nm, indicating a ductile mode cutting. However, the rake angle has a strong influence on the chip profile. Specifically, the smaller the rake angle, the less pronounced the saw-tooth characteristics of the chip, the less volume of the chip, and the less stress concentration in the vicinity of the tool edge.

At a larger DOC of 125 nm, the chips are continuous for the rake angles of − 30° and − 45°. However, there are brittle fracture of displaced base material and fracture of continuously formed chip observed for the rake angle of 0° and − 15°, indicating the dominant brittle mode cutting. In particular for

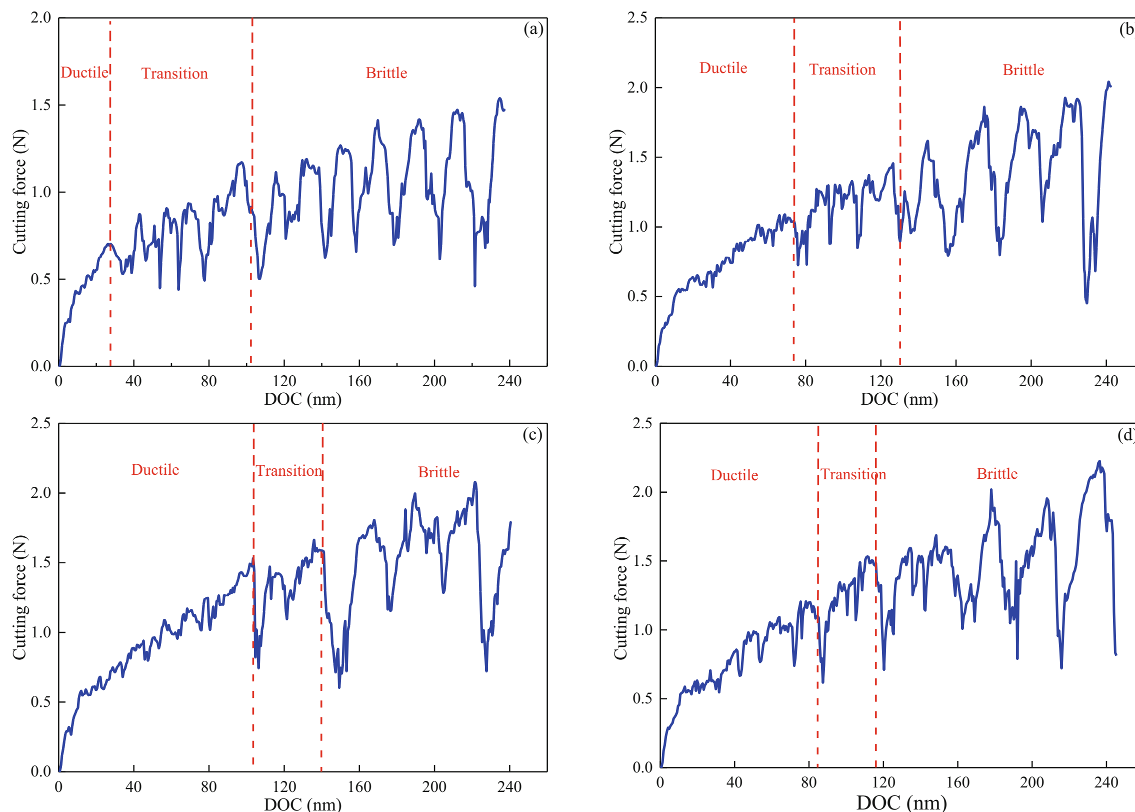

Fig. 8 Evolutions of cutting force in FE simulations of grooving using different rake angles. Rake angles are the following: **a** 0°, **b** − 30°, **c** − 45°, and **d** − 60°

the rake angle of − 60°, the formed chips accumulate into blocks, with the absence of saw-tooth characteristics. Figure 7 also indicates that the obtained machined surface is smoother and of less surface cracks for rake angles of − 30° and − 45°. For the smallest rake angle of − 60°, the continuous chip flow on the rake face of the cutting tool is seriously suppressed, and the interaction between formed chips and machined surface leads to the deterioration of machined surface quality. The as-observed rake angle dependence of the critical DOC can be attributed to the transition of dominant stress states from shear to compressive, which is conducive to the formation of hydrostatic pressure zone and thus facilitating ductile mode cutting.

Figure 8 plots the variation of cutting force with increasing of DOC in FE simulations of grooving using different rake angles. It is seen from Fig. 8 that the cutting force-DOC curve presents similar characteristics of different cutting regimes for each rake angle. And Fig. 8 also suggests that the rake angle has a strong influence on the cutting force. Firstly, the regime of ductile mode cutting increases with decreasing rake angle in the range from 0° to − 45°, after which decreases with a further decrease of rake angle from − 45° to − 60°. Secondly, a decrease of rake angle leads to an increased average cutting force in the brittle mode cutting. Thirdly, the fluctuation of cutting force is less pronounced for a smaller rake angle. Based on the investigation of chip profile and cutting force, the derived critical DOC for the BTD transition is 105, 118, 132, 140 nm, and 116 nm for the rake angles of 0°, − 15°, − 30°, − 45°, and − 60°, as listed in Table 2. Therefore, above results indicate that there is a critical rake angle of − 45° for the largest critical DOC of 140 nm for the BTD transition in diamond grooving of silicon, corresponding to the most pronounced ductile machinability of silicon.

In order to further explore the influence of rake angle on the BTD transition of silicon, FE simulations of conventional cutting using different rake angles but with a constant DOC of 70 nm are performed. Figure 9 a shows the schematic diagram of chip formation in the cutting process. The area of the primary shear zone is controlled by the shear plane length L_{AB}. The change in the rake angle of the cutting tool significantly affects the L_{AB}. As the area of the shear zone increases, the strength of the material increases and the deformation energy increases. Figure 9 b presents a typical cutting configuration by FE simulation with a rake angle of − 15°. It is obvious that

Table 2 Critical DOC for different rake angles

Rake angle	0°	− 15°	− 30°	− 45°	− 60°
Critical DOC	105 nm	118 nm	132 nm	140 nm	116 nm

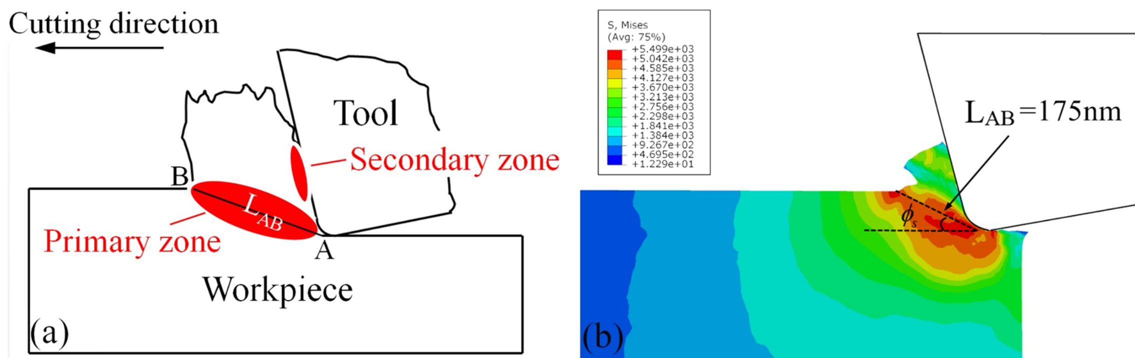

Fig. 9 Chip formation in diamond cutting of silicon. **a** Schematic illustration. **b** FE simulation

Fig. 10 Shear plane length by FE simulations of conventional cutting with a constant DOC of 70 nm. Rake angles are the following: **a** 0°, **b** − 15°, **c** − 30°, **d** − 45°, and **e** − 60°

the stress concentrated in the primary zone and the shear plane length L_{AB} is about 175 nm.

Figure 10 presents FE simulation results for each rake angle. Specifically, the measured values of L_{AB} are provided. It can be seen from Fig. 10 that both the length of shear plane and von Mises stresses increase with a decrease of rake angle in the range from 0° to − 45°. However, the length of shear plane decreases from 215 nm at the rake angle of − 45° to 205 nm at the rake angle of − 60°. These results strongly demonstrate that the hydrostatic pressure in the vicinity of cutting region is advantageous for achieving ductile mode cutting of silicon. And the distribution of pressure concentration in the cutting process is strongly affected by the rake angle of the cutting tool.

4 Summary

In summary, we establish a 2D finite element model of orthogonal cutting of monocrystalline silicon based on the DP constitutive model, which is capable of describing co-existing deformation behaviors of plastic flow and brittle fracture of silicon. Finite element simulation of grooving is performed, and the BTD transition is identified by analyzing both evolutions of chip profile and cutting force. The predicted value of critical DOC for the BTD transition of silicon for a rake angle of − 15° is 118 nm, which is of well agreement with the measured value of 121 nm from corresponding grooving experiment using the same machining parameters. Subsequent FE simulations of grooving and conventional cutting demonstrate that the critical DOC for the BTD transition is strongly dependent on the rake angles ranging from 0° to − 60°. And a critical rake angle of − 45° possesses the most pronounced ductile machinability of silicon in diamond cutting.

Funding information This work was financially supported by the National Natural Science Foundation of China (NSFC)-German Research Foundation (DFG) international joint research program (51761135106), the Science Challenge Project (Nos. TZ2018006-0201-02 and TZ2018006-0205-02), the Foundation of Laboratory of Ultra Precision Manufacturing Technology, CAEP (ZD 18007), and the Fundamental Research Funds for the Central Universities and Open Research Foundation of State Key Laboratory of Digital Manufacturing Equipment and Technology in Huazhong University of Science and Technology, China (DMETKF2018007 and DMETKF2019016).

References

1. Rajendra S (2009) Why silicon is and will remain the dominant photovoltaic material. J Nanophotonics 3:032503
2. Saoubi RM, Outeiro JC, Chandrasekaran H, Dillon OW, Jawahir IS (2008) A review of surface integrity in machining and its impact on functional performance and life of machined products. Int J Sustain Manuf 1:203–236
3. Chon KS, Namba Y (2010) Single-point diamond turning of electroless nickel for flat X-ray mirror. J Mech Sci Technol 24:1603–1609
4. Higginbottom DB, Campbell GT, Araneda G, Fang FZ, Colombe Y, Buchler BC, Lam PK (2018) Fabrication of precision hemispherical mirrors for quantum optics applications. Sci Rep 8:221
5. Gilman JJ (1993) Why silicon is hard. Science 261:1436–1439
6. Arif M, Rahman M, San WY (2012) A state-of-the-art review of ductile cutting of silicon wafers for semiconductor and microelectronics industries. Int J Adv Manuf Technol 63:481–504
7. Chen YL, Cai Y, Shimizu Y, Ito S, Gao W, Ju BF (2016) Ductile cutting of silicon microstructures with surface inclination measurement and compensation by using a force sensor integrated single point diamond tool. J Micromech Microeng 26:025002
8. Liu K, Zuo D, Li XP, Rahman M (2009) Nanometric ductile cutting characteristics of silicon wafer using single crystal diamond tools. J Vac Sci Technol B 27:1361–1366
9. Zhou M, Ngoi BKA, Zhong ZW, Chin CS (2001) Brittle-ductile transition in diamond cutting of silicon single crystals. Mater Manuf Process 16:14
10. Uddin MS, Seah KHW, Rahman M, Li XP, Liu K (2007) Performance of single crystal diamond tools in ductile mode cutting of silicon. J Mater Process Technol 185:24–30
11. Leung TP, Lee WB, Lu XM (1998) Diamond turning of silicon substrates in ductile-regime. J Mater Process Technol 73:42–48
12. Blake PN, Scattergood RO (1990) Ductile-regime machining of germanium and silicon. J Am Ceram Soc 73:9
13. Chao CL, Ma KJ, Liu DS, Bai CY, Shy TL (2002) Ductile behaviour in single-point diamond-turning of single-crystal silicon. J Mater Process Technol 127:87–190
14. Yan J, Syoji K, Kuriyagawa T, Suzuki H (2002) Ductile regime turning at large tool feed. J Mater Process Technol 121:63–372
15. Shibata T, Fujii S, Makino E, Ikeda M (1996) Ductile-regime turning mechanism of single-crystal silicon. Precis Eng 18:29–137
16. Fang FZ, Venkatesh VC (1998) Diamond cutting of silicon with nanometric finish. Cirp Ann Manuf Technol 47:5–49
17. Wu C, Li B, Yang J, Liang S (2016) Prediction of grinding force for brittle materials considering co-existing of ductility and brittleness. Int J Adv Manuf Technol 87:1967–1975
18. Yan JW, Tamaki J, Syoji K (2004) Single-point diamond turning of CaF2 for nanometric surface. Int J Adv Manuf Technol 24:640–646
19. Uddin MS, Seah KHW, Rahman M, Li XP, Liu K (2007) Performance of single crystal diamond tools in ductile mode cutting of silicon. J Mater Process Technol 185:4–30
20. Patten JA, Gao W (2001) Extreme negative rake angle technique for single point diamond nano-cutting of silicon. Precis Eng 25:65–167
21. Zhang ZY, Du Y, Wang B, Wang Z, Kang RK, Guo D (2017) Nanoscale wear layers on silicon wafers induced by mechanical chemical grinding. Tribol Lett 65:132
22. Zhang ZY, Cui JF, Wang B, Wang Z, Kang RK, Guo DM (2017) A novel approach of mechanical chemical grinding. J Alloys Compd 726:14–524
23. Xiao G, To S, Zhang G (2015) Molecular dynamics modelling of brittle-ductile cutting mode transition: case study on silicon carbide. Int J Mach Tool Manu 88:14–222
24. Zhang JG, Suzuki N, Wang YL, Shamoto E (2014) Fundamental investigation of ultra-precision ductile machining of tungsten carbide by applying elliptical vibration cutting with single crystal diamond. J Mater Process Technol 214:644–2659
25. Liu K, Li XP, Liang SY (2007) The mechanism of ductile chip formation in cutting of brittle materials. Int J Adv Manuf Technol 33:75–884
26. Yang TS, Chang SY, Chou JC (2012) Predictions of scratch characters for engineering material by using fem and abductive network. Appl Mech Mater 232:59–664

27. Zhang ZY, Guo DM, Wang B, Kang RK, Zhang B (2015) A novel approach of high speed scratching on silicon wafers at nanoscale depths of cut. Sci Report 5:16395
28. Wang B, Zhang ZY, Chang KK, Cui JF, Andreas R, Yu JH, Lin CT, Chen GX, Zang KT, Luo J, Guo DM (2018) New deformation-induced nanostructure in silicon. Nano Lett 18:4611–4617
29. Yan JW, Zhao HW, Kuriyagawa T (2009) Effects of tool edge radius on ductile machining of silicon: an investigation by fem. Semicond Sci Technol 24:075018
30. Mir A, Luo XC, Cheng K, Cox A (2017) Investigation of influence of tool rake angle in single point diamond turning of silicon. Int J Adv Manuf Technol 94:2343–2355
31. Shi LQ, Li XW, Yu F (2013) Finite element simulation of precision cutting monocrystalline silicon. Adv Mater Res 662:99–102
32. Liu HT, Xie WK, Sun YZ, Zhu XF, Wang MH (2017) Investigations on brittle-ductile cutting transition and crack formation in diamond cutting of mono-crystalline silicon. Int J Adv Manuf Technol 95:9–10
33. Wang SF, An CH, Zhang FH, Wang J, Lei XY, Zhang JF (2016) An experimental and theoretical investigation on the brittle ductile transition and cutting force anisotropy in cutting KDP crystal. Int J Mach Tool Manu 106:98–108
34. Lee SH, Ahn BW (2006) Monitoring of brittle-ductile transition during AFM machining using acoustic emission. Key Eng Mater 326–328:405–408
35. Koshimizu S, Otsuka J (2001) Detection of ductile to brittle transition in microindentation and microscratching of single crystal silicon using acoustic emission. Mach Sci Technol 5:101–114
36. Youn SW, Kang CG (2005) FEA study on nanodeformation behaviors of amorphous silicon and borosilicate considering tip geometry for pit array fabrication. Mater Sci Eng 390:233–239
37. Blaedel KL, Carr JW, Davis PJ, Goodman WA, Haack JK, Krulewich D (2001) An empirical survey on the influence of machining parameters on tool wear in diamond turning of large single-crystal silicon optics. Precis Eng 25:247–257
38. Fang FZ, Zhang GX (2003) An experimental study of edge radius effect on cutting single crystal silicon. Int J Adv Manuf Technol 22: 703–707
39. Zhao QL, Chen MJ, Liang YC, Dong S, Deng C (2002) Effects of diamond cutting tool's rake angle and rounded cutting edge radius on the machined single crystal silicon surface quality. J Mech Engen 12:54–59
40. Durazo-Cardenas I, Shore P, Luo XC, Jacklin T, Impey SA, Cox A (2007) 3D characterisation of tool wear whilst diamond turning silicon. Wear 262:340–349
41. Wang MH, Wang W, Lu ZS (2013) Critical cutting thickness in ultra-precision machining of single crystal silicon. Int J Adv Manuf Technol 65:843–851
42. Mir A, Luo XC, Siddiq A (2017) Smooth particle hydrodynamics study of surface defect machining for diamond turning of silicon. Int J Adv Manuf Technol 88:2461–2476
43. Ando T, Sato K, Shikida M, Yoshioka T, Yoshikawa Y, Kawabata T (1997) Orientation-dependent fracture strain in single-crystal silicon beams under uniaxial tensile conditions. Proc IEEE Int Symp Micromechatronics Hum Sci:55–60
44. Zhang JJ, Zhang JG, Wang ZF, Hartmaier A, Yan Y, Sun T (2017) Interaction between phase transformations and dislocations at incipient plasticity of monocrystalline silicon under nanoindentation. Comput Mater Sci 131:55–61
45. Zhu B, Zhao D, Zhao HW, Guan J, Hou PL, Wang SB, Qian L (2017) A study on the surface quality and brittle-ductile transition during the elliptical vibration-assisted nanocutting process on monocrystalline silicon via molecular dynamic simulations. RSC Adv 7:4179–4189
46. Ravindra D, Ghantasala MK, Patten J (2012) Ductile mode material removal and high-pressure phase transformation in silicon during micro-laser assisted machining. Precis Eng 36:364–367
47. Zhang ZB, Stukowski A, Urbassek HM (2016) Interplay of dislocation-based plasticity and phase transformation during Si nanoindentation. Comput Mater Sci 119:82–89
48. Callahan DL, Morris JC (1992) The extent of phase transformation in silicon hardness indentations. J Mater Res 7:1614–1617
49. Cai MB, Li XP, Rahman M (2007) High-pressure phase transformation as the mechanism of ductile chip formation in nanoscale cutting of silicon wafer. P I Mech Eng B-J Eng 221:1511–1519
50. Yan J, Asami T, Harada H, Kuriyagawa T (2009) Fundamental investigation of subsurface damage in single crystalline silicon caused by diamond machining. Precis Eng 33:378–386
51. Zhang ZY, Wang B, Kang RK, Zhang B, Guo DM (2015) Changes in surface layer of silicon wafers from diamond scratching. CIRP Ann Manuf Technol 64:349–352

Publisher's note Springer Nature remains neutral with regard to jurisdictional claims in published maps and institutional affiliations.